PROCEEDINGS of the
23rd International Congress on Acoustics
9 to 13 September 2019 in Aachen, Germany

On the impact of the shape of the artificial boundary in exterior Helmholtz problems

Nick WULBUSCH[(1)], Reinhild RODEN[(2)], Alexey CHERNOV[(1)], Matthias BLAU[(2,3)], Andrea MOIOLA[(4)]

[(1)]Institut für Mathematik, Universität Oldenburg, Germany, nick.wulbusch@uni-oldenburg.de
[(2)]Institut für Hörtechnik und Audiologie, Jade Hochschule Oldenburg, Germany
[(3)]Cluster of Excellence Hearing4All, Germany
[(4)]Department of Mathematics, University of Pavia, Italy

Abstract

Acoustic problems can be investigated numerically in the frequency domain by solving the Helmholtz equation with the finite element method (FEM). In exterior problems we approximate the radiation condition by truncating the considered domain with an artificial absorbing boundary. Popular choices include absorbing boundary conditions (ABC) or perfectly matched layers (PML), where the implementation of the latter is usually more involved. Both methods have the disadvantage (although for PML this is less significant) that they still reflect certain parts of the wave. This reflection error is typically small for normal (0 degrees) incidence but increases with larger incidence angles. In this numerical study we consider a model problem in two dimensions. For various ABCs we study the impact of changing the shape of the artificial boundary on the reflection error and the accuracy of the numerical simulations. The outcome of numerical simulations for different ABCs and methods of shape optimization are discussed in detail.

Keywords: FEM, Absorbing boundary conditions, Helmholtz equation

1 INTRODUCTION

Solutions to exterior Helmholtz problems, which arise often in acoustics and electromagnetics, can be approximated in a truncated domain via the finite element method. The truncation leads to additional errors, which depend largely on the method that is used to approximate the Sommerfeld radiation condition [8, 6, 5]. Many tools have been proposed to deal with this problem, like perfectly matched layers [3, 9, 6], the Dirichlet-to-Neumann-operator [6] and local absorbing boundary conditions [1, 2]. In this study we further investigate some of the latter, more precisely the impedance boundary condition and the curvature absorbing boundary condition (C-ABC). These boundary conditions are quite well understood [1, 6, 7, 2] and often used on a circular/spherical truncation domain in 2D/3D. Further they lead to large errors, if the "angle of incidence" of the wave is large. "Angle of incidence" is meant to be the angle between a suitably defined Poynting vector and the normal vector at the boundary. In this study we will consider a model problem in 2D and change the artificial boundary in order to find a truncation that leads to improved accuracy.

2 MODEL PROBLEM

Consider the following exterior Dirichlet problem (1)

$$\begin{aligned} -\Delta p - k^2 p &= 0 \quad \text{in } \Omega \\ p &= p_D \quad \text{on } \Gamma_D \\ \lim_{|x|\to\infty} |x|^{\frac{1}{2}} \left(\frac{\partial p}{\partial |x|} - ikp \right) &= 0 \end{aligned} \tag{1}$$

where $\Omega \subset \mathbb{R}^2$ is the complement of a bounded domain and Γ_D its boundary. p denotes the (complex) pressure and k is the wavenumber. In this study we will look at approximations of this problem by truncating the

boundary. To deal with the Sommerfeld radiation condition we use two different boundary conditions, which are briefly introduced in the next subsection.

2.1 Boundary Conditions

In this section we introduce the boundary conditions to approximate the Sommerfeld radiation condition used in this study. To do so we truncate the infinite domain by an artificial boundary Γ_+. We follow the derivation in [1] and compare two different absorbing boundary conditions.

2.1.1 Impedance boundary condition

The simplest boundary condition is the impedance boundary condition. Here we enforce

$$\frac{\partial p}{\partial n} - ikp = 0 \text{ on } \Gamma_+, \tag{2}$$

where $\frac{\partial p}{\partial n}$ denotes the normal derivative (pointing outwards) of p. This boundary condition perfectly absorbs a planar wave that hits the boundary perpendicularly. In exterior problems the scattered field is not a planar wave, so that in practice this boundary condition leads to errors. However, if we place the artificial boundary far away from the obstacle, we actually get a good approximation to the Sommerfeld radiation condition. The large distance required between the scatterer and the truncation boundary may lead to significant computational cost and should therefore be avoided.

2.1.2 C-ABC

Following [1, eq.(3.14)] we arrive at another approximation for the Sommerfeld radiation condition, assuming the angle of incidence is small[1]:

$$\frac{\partial p}{\partial n} - ikp + \left(\gamma + \frac{\kappa}{4}\right) p + \left(\gamma - \frac{\kappa}{4}\right) \frac{1}{ik} \frac{\partial p}{\partial n} = 0 \text{ on } \Gamma_+, \tag{3}$$

where κ is the curvature of Γ_+ and γ is a parameter that can be chosen freely. In the numerical experiments in [1] it was shown that the value of γ did not have much influence, so (as also described in [1], see also [2]) for the sake of simplification we assume $\gamma = \frac{\kappa}{4}$ and arrive at the so called curvature absorbing boundary condition (C-ABC):

$$\frac{\partial p}{\partial n} - ikp + \frac{\kappa}{2} p = 0 \text{ on } \Gamma_+. \tag{4}$$

2.2 Shape deformation

Since the standard impedance boundary condition is exact for perpendicular incoming planar waves, we expect that it approximates a non-planar wave better when this hits the boundary perpendicularly. We propose to estimate the main direction of propagation of p by the Poynting vector $\Re(\frac{\bar{p}\nabla p}{ik})$ or alternatively by the gradient of the complex argument $\arg(p)$, since a simple calculation reveals

$$\Re(\frac{\bar{p}\nabla p}{ik}) = c(p,k)\nabla \arg(p), \tag{5}$$

for some scalar c, so the vectors in both expressions point into the same direction (except for the discontinuity jumps of $\arg(p)$ from π to $-\pi$). Therefore the estimated main direction of propagation is perpendicular to a contour line of $\arg(p)$. For the sake of a fair comparison we want to fix the area of the domain, such that the computational cost does not change significantly (we will get roughly the same number of elements). Hence in the numerical experiments we will consider a contour line that encloses nearly the same area as the nominal circle and consider the interior as the new computational domain.

[1] Notice that the sign in front of ikp is modified according to the sign convention in the time-harmonic ansatz from [1]

3 NUMERICAL SIMULATIONS

In this section we present some numerical results that could be observed with shape deformation. In the following experiments we have wavenumber $k = \frac{\omega}{c}$ with angular frequency $\omega = 2\pi f$, frequency f and speed of sound $c = 343\frac{m}{s}$. The spatial dimensions are given in meter (m).

3.1 Model problem I: Scattering

The first model problem we are looking at is a standard scattering problem of the following form

$$\begin{aligned} -\Delta p - k^2 p &= 0 && \text{in } \Omega \\ p &= -p_{inc} && \text{on } \Gamma_D \\ \lim_{|x|\to\infty} |x|^{\frac{1}{2}} \left(\frac{\partial p}{\partial |x|} - ikp \right) &= 0 \end{aligned} \tag{6}$$

where p_{inc}, defined in polar coordinates (r, θ),

$$p_{inc} = p_0 e^{ikr\sin(\theta_{inc}-\theta)} \tag{7}$$

is the incoming (planar) wave hitting the obstacle from the right, i.e. (following the convention in [4]) $\theta_{inc} = \frac{3}{2}\pi$, and amplitude $p_0 = 1$. Here Γ_D describes the boundary of a circle, the scatterer, with radius a and Ω is the exterior of this scatterer. The analytic solution (see [4]), i.e. the scattered acoustical field, of this problem is given (in polar coordinates) by

$$p(r,\theta) = -p_0 \sum_{n=-\infty}^{\infty} \frac{J_n(ka)}{H_n^{(1)}(ka)} H_n^{(1)}(kr) e^{in(\theta_{inc}-\theta)}, \ r \geq a, \tag{8}$$

where $p_0 = 1$, $\theta_{inc} = \frac{3}{2}\pi$, J_n denotes the Bessel function of the first kind of order n and $H_n^{(1)}$ denotes the Hankel function of first kind of order n.

In our experiments we truncate the infinite domain by different artificial boundaries and solve the corresponding problem (9) with standard quadratic finite elements on that finite domain, where we use different approximations for the Sommerfeld radiation condition:

$$\begin{aligned} -\Delta p - k^2 p &= 0 && \text{in } \Omega \\ p &= -p_{inc} && \text{on } \Gamma_D \\ \mathscr{B}(p) &= 0 && \text{on } \Gamma_+, \end{aligned} \tag{9}$$

where $\mathscr{B}(p)$ denotes one of the conditions (2) or (4). We choose $a = 0.5\,\text{m}$ for the radius of the scatterer.

3.1.1 Truncated domains

For the numerical simulations we used two different domains with the following boundaries:

(1) Circle with radius 1.5 m, see figure 1

(2) Contour line of $\arg(p)$, see figure 2

The boundary of the contour domain is generated with the help of `Matlabs contour`-function on the analytic solution with $f = 1000\,\text{Hz}$. The shape of the contour lines does not vary much with the frequency. For low frequencies however, for which the wavelength is much larger than the diameter of the domain, there is no contour line of $\arg(p)$ that could be used as boundary for the truncated domain, such that the area remains approximately the same. Thus, for lower frequencies ($< 150\,\text{Hz}$) the angles of incidence are not necessarily close to 0.

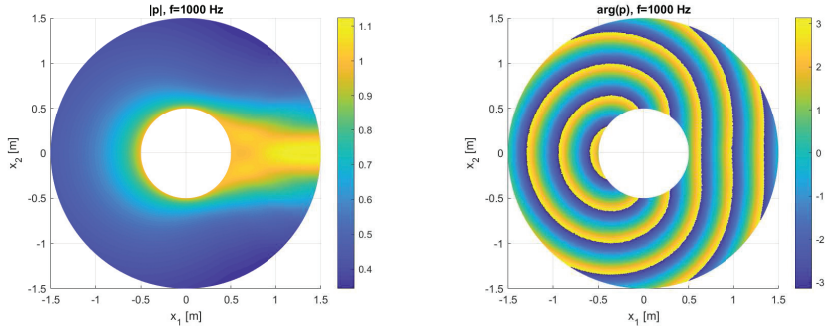

Figure 1. $|p|$ and $\arg(p)$ in circular domain, $f = 1000\,\mathrm{Hz}$

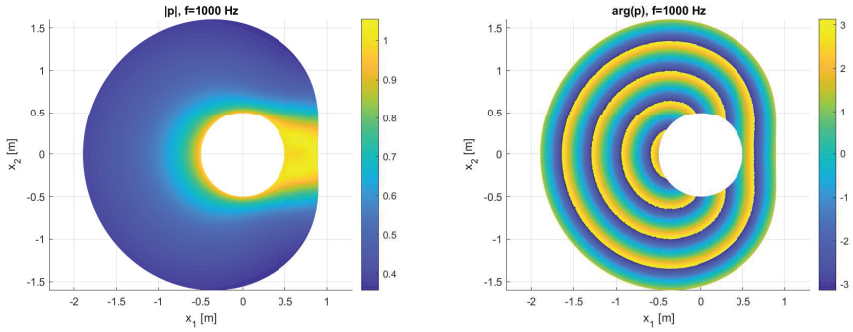

Figure 2. $|p|$ and $\arg(p)$ in contour domain, $f = 1000\,\mathrm{Hz}$

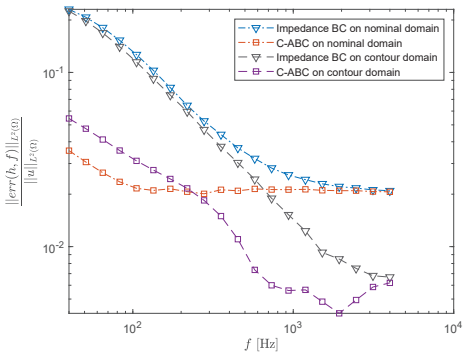

Figure 3. Relative L^2-error as a function of frequency f for a fixed mesh ($h \approx 0.0118$, #(degrees of freedom) $\approx 4.5 \times 10^5$, 7 elements per wavelength for largest frequency) for the circular scattering problem.

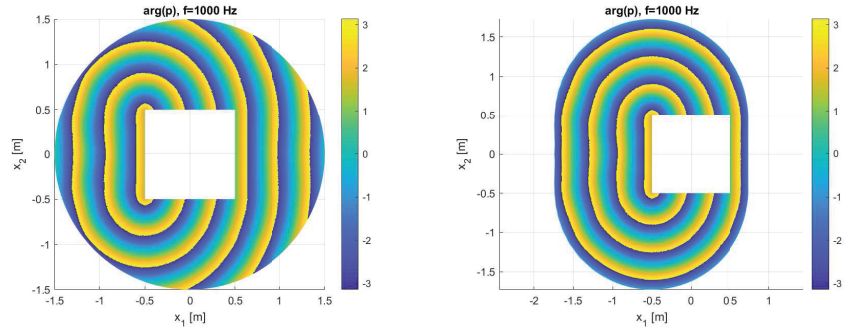

Figure 4. $\arg(p)$ in circular domain (left) and contour domain (right), $f = 1000\,\text{Hz}$

3.1.2 Results

We compare the relative error in L^2-norm for the whole domain

$$\text{err}(h,f) = \frac{\|p_{FEM} - p_{exact}\|_{L^2(\Omega)}}{\|p_{exact}\|_{L^2(\Omega)}}, \tag{10}$$

where h denotes the mesh width, i.e. the maximal edge length of a triangular element of the mesh. Figure 3 shows the error for the impedance boundary condition and for the C-ABC in the nominal (circular) and contour domain. The C-ABC performs better than the impedance boundary condition. For the impedance boundary condition the error is smaller on the contour domain than on the nominal one. For the C-ABC this effect only takes place for frequencies higher than 200 Hz. Notice that the mesh is fixed, i.e. solutions for higher frequencies might still improve from mesh refinement, while for the solutions for lower frequencies the model error due to the approximation of the Sommerfeld radiation dominates. From a practical stand point this is a reasonable comparison, since for many problems we cannot refine the mesh till the discretization error is below a certain threshold due to the increasing computational cost and choose the mesh size according to some "rule of thumb", such as 6 or 10 elements per wave length [6].

3.2 Different shape of scatterer

To validate the method, we look at a second scattering problem. This problem is identical to the previous one, except that now the scatterer is polygonal, to be precise a square with vertices $(-0.5,-0.5),(0.5,-0.5)$, $(0.5,0.5)$ and $(-0.5,0.5)$. No analytic solution is known for this problem. As reference solution we take a PML solution on a larger domain. The argument of the solution $\arg(p)$ can be seen in figure 4 for the nominal domain and the contour domain. The error is shown in figure 5. We can observe a similar behavior as in the previous problem.

3.3 Model problem II: Point sources

Finally we will take a look at another model problem, that generates a solution with a slightly more complicated contour line of $\arg(p)$. We consider equation (1) with p_D as a sum of 50 Hankel functions $H_1^{(0)}$ with center at $(0, 0.4 - \frac{0.8}{49}(n-1))$, $n = 1,\ldots,50$, i.e. an linear array of point sources on the y-axis from -0.4 to 0.4. The modulus of the solution $|p|$, as well as $\arg(p)$ are shown in figure 6 for $f = 2000\,\text{Hz}$. The resulting truncated contour domain is visualized in figure 7 (left). For this problem the shape of the contour lines of $\arg(p)$ largely depends on the frequency. We consider $f = 2000\,\text{Hz}$ for generating the contour domain, but still compare the error for other frequencies. Here the results do not improve for the contour domain and are only similar for high frequencies. Even for $f = 2000\,\text{Hz}$ the contour domains performs worse than the nominal one. This might be due to the non-convexity, numerical inaccuracies in the computation of the contour line and in the computed

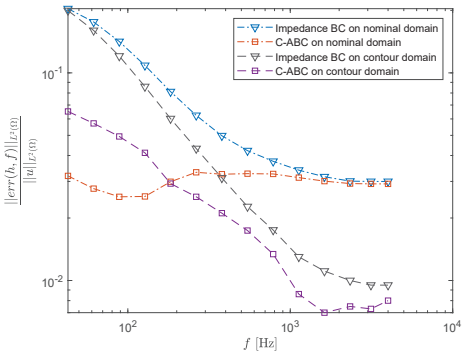

Figure 5. Relative L^2-error as a function of frequency f for a fixed mesh ($h \approx 0.0118$, #(degrees of freedom) $\approx 4.5 \times 10^5$, 7 elements per wavelength for largest frequency) for the polygonal scatterer problem.

curvature κ in case of the C-ABC. A simpler, convex domain is considered: An ellipse that is as close as possible to the contour line in the L^2-sense. We compute the parameters of this elliptic domain by solving the optimization problem (12) considered in the next subsection.

3.3.1 Ellipse optimization

The contour line will be approximated by an ellipse, parameterized via

$$f(x,y) = (x_0 + a\cos(\theta)\cos(\varphi) - b\sin(\theta)\sin(\varphi), y_0 + a\sin(\theta)\cos(\varphi) - b\cos(\theta)\sin(\varphi)) \tag{11}$$

where (x_0, y_0) denotes the center of the ellipse, a and b the semiaxes' lengths, φ the rotation of the ellipse around its center and $\theta := \theta(x,y)$ is the azimuth variable.

We solve the following optimization problem numerically

$$\min_{x_0,y_0,a,b,\varphi} \left\| \gamma(\theta) - f(x_{op}(x_0,a,b,\varphi;\theta), y_{op}(y_0,a,b,\phi;\theta)) \right\|_{L^2([0,2\pi])}$$
$$\text{such that} \quad \begin{aligned} x_{op} &= x_0 + a\cos(\theta)\cos(\varphi) - b\sin(\theta)\sin(\varphi) \\ y_{op} &= y_0 + a\sin(\theta)\cos(\varphi) - b\cos(\theta)\sin(\varphi) \end{aligned} \tag{12}$$

Here γ denotes the parametrization of the contour line with respect to θ. x_0, y_0 and φ are included, even though it is obvious that we will get $x_0 = y_0 = \varphi = 0$ up to machine precision due to symmetry. We solve this problem numerically by the gradient descent method, where we initialize $a = 1.5 = b$, $x_0 = 0 = y_0$ and $\varphi = 0$, i.e. a circle with radius 1.5 m centered at the origin (so it is equal to the nominal domain). The algorithm returns $a = 1.395$ and $b = 1.579$. The resulting domain can be seen in figure 7 (right). For this elliptic domain the error decreases for some frequencies, see figure 8. The impedance boundary condition behaves similar on all domains for low frequencies, but performs better for the elliptic domain for high frequencies. For low frequencies C-ABC performs best for the nominal domain, for high frequencies the elliptic domain is slightly superior in accuracy.

4 CONCLUSIONS

In this numerical study we compared two simple absorbing boundary conditions on different shapes of domains. We showed that deforming the shape of the artificial circular boundary, such that the angle of incidence of the wave is normal to the boundary, can improve numerical results. This was especially recognizable for higher frequencies and for the impedance boundary condition. This also indicates that the shape deformation is more

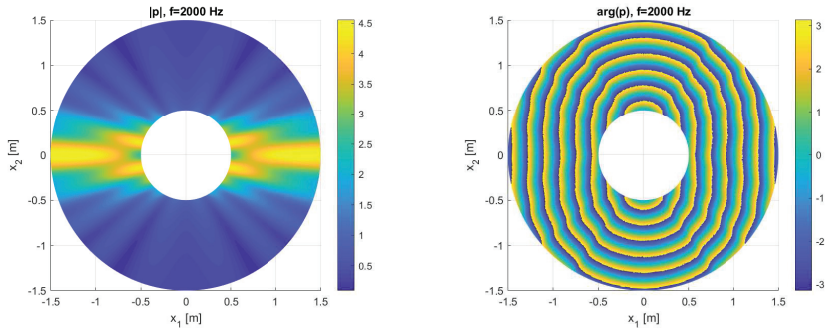

Figure 6. $|p|$ and $\arg(p)$ in circular domain, $f = 2000\,\mathrm{Hz}$

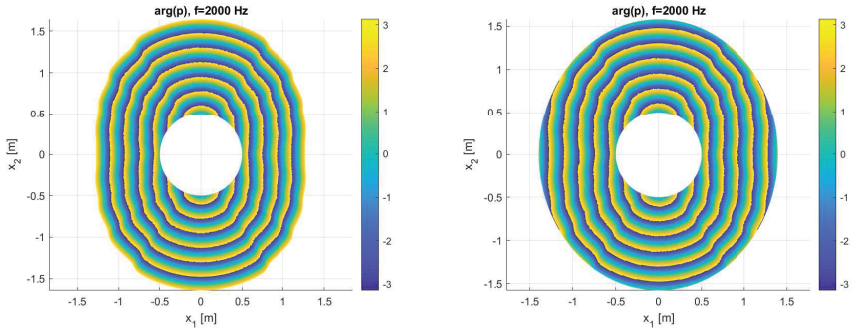

Figure 7. $\arg(p)$ in contour domain (left) and in optimized elliptic domain (right), $f = 2000\,\mathrm{Hz}$

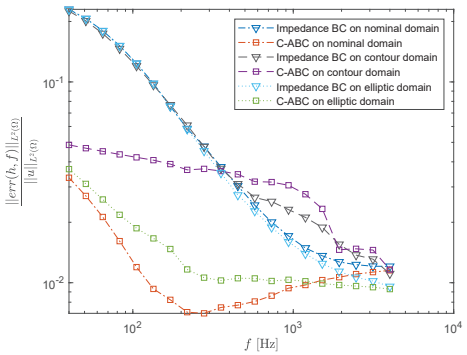

Figure 8. Relative $L^2(\Omega)$-error as a function of frequency f for a fixed mesh ($h \approx 0.0120$, #(degrees of freedom) $\approx 4.5 \times 10^5$, 7 elements per wavelength for largest frequency) for the point source problem

useful for simpler boundary conditions, since more involved conditions already deal better with some range of angles of incidence. Some problems, however, do not yield improved accuracy by using a contour domain.

5 OUTLOOK

In this study we used contour lines of the exact solution as boundary for new domains. Usually the exact solution is not known and hence a contour line can only be constructed by a numerical solution. Since solving the problem on a larger domain first and then truncating it is not necessarily reasonable, one could implement an algorithm that starts with a circular domain and changes it iteratively to a domain that is similar to the contour domain discussed above. One could further consider higher order absorbing boundary conditions and see at which order the improvement of deforming the domain vanishes. The transition to 3D problems is possible, but leads to high computational cost.

ACKNOWLEDGEMENTS

Partially funded by the Deutsche Forschungsgemeinschaft (DFG, German Research Foundation) – Projektnummer 352015383 – SFB 1330 C1.

REFERENCES

[1] Barucq, H.; Bergot, M., Chabassier, J., Estecahandy, E. Derivation of high order absorbing boundary conditions for the Helmholtz equation in 2D. [Research Report] RR-8632, INRIA, Bordeaux; INRIA. 2014. <hal-01085180>

[2] Bayliss, A.; Gunzburger, M.; Turkel, E. Boundary conditions for the numerical solution of elliptic equations in exterior regions. SIAM J. Appl. Math., vol 42, pp 430–451, 1982.

[3] Bérenger, J. A Perfectly Matched Layer for the Absorption of Electromagnetic Waves. J. Comput. Phys. 114 (2), pp. 185–200, 1994

[4] Bourlier, C.; Pinel, N.; Kubické, G. Method of Moments for 2D Scattering problems: Basic concepts and applications. John Wiley & Sons 2013. 10.1002/9781118648674.

[5] Colton, D.; Kress, R., Integral Equation Methods in Scattering Theory. New York et al., John Wiley & Sons 1983

[6] Ihlenburg, F. Finite Element Analysis of Acousting Scattering. Springer, New York, 1998.

[7] Melenk, J. M.; Sauter, S. Wavenumber explicit convergence analysis for Galerkin discretizations of the Helmholtz equation. SIAM Journal on Numerical Analysis, vol. 49, no. 3/4, 2011, pp. 1210–1243.

[8] Sommerfeld, A. Partial Differential Equations in Physics, Academic Press, New York, 1949.

[9] Turkel, E.; Yefet, A. Absorbing PML boundary layers for wave-like equations. Appl. Numer. Math. 27 (4), pp. 533–557, 1998